Enhancing the Photo-corrosion Resistance of ZnO Nanowire Photocatalysts

Caitlin M. Taylor,[a,b] Anyela Ramirez-Canon,[a,b] Jannis Wenk,[b,c] and Davide Mattia[a,b*]

[a]Centre for Sustainable Chemical Technologies, University of Bath, BA27AY, UK
[b]Department of Chemical Engineering, University of Bath, BA27AY, UK
[c]Water Innovation and Research Centre, University of Bath, BA27AY, UK

ABSTRACT

Zinc oxide (ZnO) displays superior properties as a photocatalyst, compared to the more widely used TiO_2. However, widespread application of ZnO is hampered by its high photo-corrosion in aqueous environments under UV irradiation. A systematic investigation of the effect of (i) post-production annealing, (ii) dissolved oxygen levels during photocatalysis and (iii) reactor configuration on the stability and photocatalytic activity (PCA) of ZnO nanowires, grown on either flat or circular supports, was conducted. Results show, for the first time, that it is possible to significantly enhance the photo-corrosion resistance of ZnO in water under UV irradiation while also increasing PCA. Oxygen plasma post-annealing of ZnO nanowire films led to a 46% higher photocatalytic degradation of phenol compared to as-produced films. In oxygen-saturated solutions, both thermally and oxygen plasma annealed ZnO revealed similar photo-corrosion resistance. Switching from a batch to a flow-through reactor, tripled phenol photodegradation under the same irradiation conditions from 19 to 57% due to enhanced mass transfer, while significantly increasing the stability and re-usability of the ZnO, with 5 repeat uses over 3 days showing no decrease in PCA. These results pave the way to more widespread use of photo-corrosion resistant ZnO in the degradation of organic pollutants in water.

Keywords: zinc oxide; photocatalysis; flow reactor; photo-corrosion; phenol; anodization

* Corresponding author e-mail: d.mattia@bath.ac.uk

1. Introduction

Zinc oxide (ZnO) is an attractive material for photocatalytic applications due to a combination of high excitonic stability, a direct band gap of 3.2 eV, high electron mobility, good transparency and strong luminescence at room temperature [1]. As such, ZnO has been used in a wide range of applications from water treatment [2, 3] to solar cells [4-6]. Under UV irradiation, ZnO has been successfully used to degrade organic pollutants including aromatic [7] and phenolic compounds [8], and dyes [9], in many cases outperforming TiO_2 [10]. Furthermore, ZnO can absorb visible light over a wider range of the solar spectrum compared to TiO_2 [11], resulting in the full degradation of multiple organic compounds under visible light [12, 13]. Despite these superior properties, the use of ZnO in wastewater treatment is severely limited by its instability in water, attributed either to the formation of $Zn(OH)_2$ in aqueous solutions [14], or to changes in morphology from the use of its molecular oxygen during photocatalysis [15]. Furthermore, due to its amphoteric properties, ZnO can be dissolved in both acidic (forming metal cations) and in alkaline solutions (forming oxyanions of Zn such as zincates) [16]. Environmental factors such as UV irradiation, pH of the solution, dissolved oxygen level and material properties, such as morphology and stability, have a significant effect on the stability of ZnO during photocatalysis. UV light accelerates the dissolution of ZnO in aqueous environments [17], due to the residual photo-generated holes on the ZnO surface that are able to attack the Zn-O bond, dissociating Zn^{2+} as summarized in Eq. 1a-c [16]:

photocatalysis: $ZnO_{(s)} + h\nu \rightarrow ZnO_{(s)} + h^+ + e^-$ (Eq. 1a)

re-combination: $h^+ + e^- \rightarrow h\nu$ (Eq. 1b)

photo-dissolution: $ZnO_{(s)} + 2h^+ \rightarrow Zn_{(aq.)}^{2+} + \frac{1}{2}O_2$ (Eq. 1c)

Higher intensities of incident light produce higher ZnO dissolution rates, due to the relationship between the number of electron-holes and the number of photons that reach the ZnO surface which, in turn, is proportional to the light intensity [16]. The photo-corrosion of ZnO thin films is strongly dependent on pH, with minimum dissolution around pH = 10 and maxima at both very high and very low pH values [16]. Dissolved oxygen levels also play an important role in the photo-corrosion of ZnO, since in oxygen-poor conditions, progress of the photocatalytic reaction drives molecular oxygen out of the ZnO catalyst, leading to structural erosion [18]. An oxygen-rich environment, on the other hand, preserve the original ZnO catalyst structure at the nanoscale [15].

The development of different methods for fabrication of ZnO nanostructures, including chemical vapour deposition [19], epitaxial growth [20], and electrochemical methods [9, 21, 22], has opened the possibility of improving the photo-response and stability of ZnO by controlling the material's physicochemical properties via structuring at the nanoscale [23]. For instance, it has been shown that the dissolution rate of ZnO is dependent on its particle size [24]. For ZnO nanostructured films, it has been reported that the photo-corrosion of ZnO layers immersed in a 3.5% NaCl solution and exposed to white light (130 mW/cm^2) decreased as the oxide thickness increased.[14] Modification of the ZnO lattice by doping with a range of elements such as C [25], Fe [26], Nd [27], Co [28], Cu [29], and Al [30], also improved the photocatalytic activity of zinc oxide nanostructures, albeit without any significant increase in stability. Post-treatment processes, such as thermal or surface plasma treatments have also been used to improve specific properties of ZnO but not its resistance to photo-corrosion. For example, thermal annealing at 400 °C in inert and oxygenated environments led to increased optical transparency as well as increases in electrical resistivity [31]. Similarly, it was shown that annealing (30 minutes, 250 °C) of ZnO nanowire arrays, produced via anodization of zinc foil using aqueous potassium bicarbonate ($KHCO_3$(aq)) electrolytes, could change their reflectance spectra in UV and visible light [32]. Annealing of anodized ZnO nanowire arrays (also at 250 °C) showed a 10-fold increase in photo-response across the visible range [33]. Hydrogen plasma was used to enhance the thermal stability of ZnO thin films [34], and the photo-response of Al-doped ZnO nanorod arrays [35]. Oxygen plasma was also used to improve optical detection properties of thin ZnO epitaxial films [36, 37], and the wetting behaviour of ZnO nanorod arrays [38], as well as the electrical and optical properties of Ga-doped ZnO thin films [39].

Although these studies have improved the understanding of the material and process factors affecting ZnO photo-corrosion stability, no studies, to the authors' knowledge, have focused on improving the photo-corrosion resistance of the ZnO nanostructures themselves.

In the present work, the effect of (i) post-production annealing conditions (thermal and plasma), (ii) dissolved oxygen levels during photocatalysis (atmospheric and saturated) and (iii) reactor configuration (batch or flow) on the stability and photocatalytic activity of ZnO nanowire films has been investigated.

2. Materials and Methods

2.1 ZnO nanowire film fabrication

ZnO nanowire films were produced via the electrochemical anodization of zinc foil and zinc wire to

obtain ZnO-F and ZnO-W nanowire structures, respectively.

Fabrication of ZnO-F: High purity zinc foil (99.98%, 0.25 mm thickness, Alfa Aesar) was pre-annealed in air at 300 °C (CWF1100, Carbolite) for one hour at 1 ˚C/min, followed by cleaning with acetone (HPLC grade, 99.5+%, Fisher) in an ultrasonic bath for 10 minutes. Anodization was performed in a 2-electrode cell with 8 mm spacing, using the zinc foil as the anode and stainless steel (SS316 grade) as the cathode. ZnO nanostructured films were obtained with $KHCO_3$ [0.01M] as electrolyte applying 1 V provided by a DC power supply (Agilent E3634A) for 1 hour. The temperature of the electrolyte was kept constant throughout anodization at 10 °C using a water-cooled bath (Thermo Scientific HAAKEC 10-K10, DC10-K20 or DC50-K35). After anodization, the samples were thoroughly rinsed with ethanol and deionized water and left to dry at room temperature. Details about the relationship between anodization process parameters and the morphology of the ZnO nanostructures produced can be found elsewhere [21, 22].

Fabrication of ZnO-W: ZnO nanowire-coated zinc wires were prepared by adapting the above method to a bespoke wire anodization setup (Fig. S1): Zinc (Zn) wires (Goodfellows ZN005131, diameter = 1 mm, purity = 99.9%) were cut to 35 cm length, and manually cleaned with acetone and ethanol to remove oil and grease. No electropolishing was performed. The anodization was conducted using an annular electrode system, with the zinc wire as the anode within a steel cathode tube connected directly to a DC power supply (1.5V). Potassium bicarbonate ($KHCO_3$, 0.05M) in ultrapure water was circulated as the electrolyte. The temperature of the electrolyte was kept constant at 8 °C during anodization using a water-glycerol cooling system (Agilent). The anodization times ranged from 5-15 minutes at 5-minute intervals, and 30-60 minutes at 15 minute intervals.

2.2 Post-annealing

Both ZnO-F and ZnO-W films were exposed to thermal annealing at temperatures ranging from 200 to 350 °C and for 1 to 72 hours in air with a 1 ˚C/min ramp. Films annealed with oxygen plasma were placed for 20 minutes in the chamber of a Diener plasma generator with a power of 50 W, oxygen flow rate of 50 mL/h at 2 bar and at room temperature.

Subsequently, the annealed films were stored in darkness in a desiccator cabinet until use.

2.3 ZnO nanowire film characterisation

The surface morphology of the ZnO nanowire films was studied using a JEOL 6301F field emission scanning electron microscope (FESEM) equipped with an energy dispersive X-ray spectrometer (EDX, Oxford, ONCA x-ray analyser, Oxfordshire, UK). The films' crystal structure was investigated using an X-ray diffractometer (Philips Xray generator – PW 1710; flat plate mode; 2θ values from 0° to 100°) and a transmitted electronic microscopy (Philips CM200 FEGTEM Field emission gun TEM/STEM) fitted with a supertwin Objective lens, cryo-shielding (Oxford Instruments) and UTW EDX detector running ISIS software and Gatan GIF200 Imaging Filter for EELS/EFTEM. Composition analysis was carried out through X-Ray Photoelectron Spectroscopy (*XPS* - GV Escalab 250) equipped with a high intensity monochromated Al Kα source, focused to a spot 120-600 μm in diameter on the sample surface.

2.4 Photocatalytic experiments

Phenol was selected as a model compound to measure the photocatalytic activity (PCA) of ZnO due to its well-characterized photodegradation pathway [40]. PCA reactions were studied in unbuffered ultrapure water (18.2 MΩ·cm, PURELAB®, ELGA LabWater) at 50 or 80 mL volume of solution with phenol (5 or 10 ppm) at 10 ± 1 ˚C in a batch recirculating reactor, consisting of a jacketed vessel of 100 mL (reservoir) with a magnetic stirrer (1000 rpm) where temperature was controlled using a water-cooled bath (Thermo Scientific), under two distinct configurations (Fig.1a):

Configuration I for ZnO-F: The ZnO-F film was placed inside the vessel on an open superstructure above the stir bar. UV light was provided from the top at a fixed distance of 3 cm between the solution and the UV-lamp (UVG-54 Handheld UV lamp, 254 nm, 6W) with an intensity of light of 0.90 ± 0.01 mW/cm^2, measured using a UV light meter (HHUV254SD – OMEGA engineering).

Configuration II for ZnO-W: PCA experiments were carried out using an in-house designed flow-through reactor (Fig.1b) consisting of three UV lamps (UVH101, Pisces, 254 nm, 5W) evenly spaced at a distance of 5 cm around a central quartz glass tube (OD = 5 mm, ID = 4 mm, light intensity 11.95 ± 0.01 mW/cm^2) containing the ZnO-coated zinc wire and the recirculating model contaminant solution. The recirculating flow rate was varied between 100 mL and 570 mL min^{-1}.

In a previous publication [40], the batch reactor was optimized to ensure that (i) the stirring speed was sufficiently high to ensure that data was collected in the kinetic regime, with no influence on photocatalytic degradation arising from mass transfer limitations; (ii) the effect of photolysis was less than 5% of the total degradation of phenol [41]; and (iii) although complete mineralization of the phenol required up to 12 hours, recording of the changes occurring in the first 4 hours was sufficient to establish a clear relation between

changes in material properties and their effect on the films' photocatalytic degradation activity [40].

Photocatalytic experiments were performed either in unsaturated DO conditions, obtained by natural absorption of oxygen from the environment in the open batch reactor or in saturated oxygen, obtained by saturating the reaction solution with oxygen (100 mL/min) for 20 minutes before, and continuing during the experiment. Before and after each experiment, the reactor system was rinsed with 250 mL pure water.

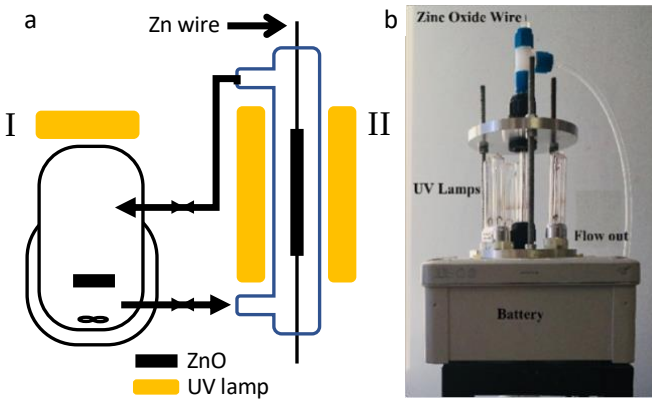

Fig. 1. a) Schematic of the two-configuration reactor used to test the photocatalytic activity of both ZnO-F (configuration I) and ZnO-W (configuration II) nanowires. Differences in light emission intensity have been calculated for each reactor to compare results. b) Photograph of the configuration II reactor.

2.5 Analysis

To determine phenol degradation, samples of 1 mL were withdrawn during irradiation at different times and then filtered using a PVDF Millex-VV Syringe Filter Unit (pore size: 0.1 µm, diameter: 33 mm). The samples were sufficiently small avoid any significant changes in the phenol concentration, ensuring reproducibility. Changes in concentration of phenol and its products were measured by HPLC using either Shimadzu SCL-10A or Agilent 1200 machines equipped with 150 mm x 2.0 mm, (Thermo, Germany) and 50 mm x 4.6 mm (Poroshell 120, 2.7 µm, Nacalai Tesque, Japan) reverse phase C18 columns, respectively. The full degradation pathway of phenol using ZnO nanowires was studied in a previous publication [40].

Isocratic mobile phase conditions were 20-25% acetonitrile and 75-80% water with 5 mM phosphoric acid (pH 2) at flow rate of 0.5-1.0 mL/min. UV detection was set to 220 nm [42]. Additional measurements such as pH, conductivity and dissolved oxygen (DO) were conducted using a bench top multi-parameter meter (Versa-Star®). Measurements of dissolved zinc were carried out by atomic absorption spectroscopy (Perkin Elmer Analyst 100) using air-acetylene with a flow of 7-10 mL/min, and by ICP-MS (Thermo Fisher Scientific ELEMENT 2XR), with 1 mL samples prepared using 0.25 mL reaction solution and 0.75 mL of Ultrapure water, then diluted to 6.25 mL and spiked 3% HNO_3 (a factor of 6.25).

To enable comparison between the two irradiation systems, PCA results were normalised to account for the different light intensity. This was considered by presenting degradation data as a function of UV dose (mJ/cm^2), rather than reaction time. UV dose was calculated by multiplying the time the solution was exposed to UV light by the effective light intensity of the system [43]. In the case of configuration I, this required subtracting the intensity of light absorbed by the medium. For configuration II, absorption by the medium was negligible due to the thin liquid layer surrounding the ZnO=W; however, due to the continuous nature of this configuration, the results had to be normalised by the fraction of solution volume receiving the dose at any given time. Details of the calculations are provided in Table S1.

3. Results and Discussion

Anodization using $KHCO_3$ electrolytes produced nanowire structures, in agreement with literature results [32]. In previous publications, the authors have shown (i) how anodization process parameters (voltage, electrolyte type and concentration, temperature and time) determine the films' morphology [21, 22]; and (ii) how this then affects the photocatalytic activity of the nanowire films, by determining crystal structure, nanowire shape and light absorbance [40]. The formation of the nanowire structures is the result of competition between the formation of Zn ion complexes (Zn^{2+}) that oxidise into ZnO, and an etching process that dissolves the formed ZnO layer [21]. Some of the Zn(II) soluble species produced during the dissolution of Zn and ZnO can react with dissociated ions from the electrolyte (i.e. HCO_3^-) to form salt or Zn complexes. Some of these ions are deposited on the surface while others are attracted to the electrodes and incorporated into the newly formed layers of ZnO. The latter phenomenon has been observed during the formation of alumina via anodization [44].

XPS analysis showed that the main components of the as-produced films were Zn (34%) and O (55%), with traces of other compounds (C and Fe). The carbon atoms are likely the result of incorporation into the nanowire structure of electrolyte ions, well documented in the case of anodic alumina nanostructures [45], while the iron is attributed to post-synthesis contamination of the samples used for analysis.

XRD analysis of the as-produced ZnO nanowire structures showed they contained some wurtzite-type crystals (Fig. 2). Annealing at temperatures ranging from

200 to 350 °C for 1h showed a progressive increase in ZnO peaks with no further change observed beyond 350 °C. Longer annealing times at 350 °C (up to 24h) showed marginal increases in the ZnO peaks, while further annealing up to 72h produced no further change in XRD patterns (not shown). For thermal treatment, the increase in the intensity of the ZnO (100), (002) and (101) peaks revealed that the material became more crystalline after treatment; additionally, the peaks become broader indicating an increase in the grain size [46, 47]. An overlap of the (101) ZnO peak with the (002) Zn peak occurred, limiting the analysis of the preferential orientation of the crystallites. These results agree with other studies on ZnO produced via anodization [31, 48, 49]. For the plasma annealed films, changes in crystallinity were less pronounced: although ZnO peaks increased and became broader, the intensity of the ZnO (100) and (002) peaks was lower compared to the thermally annealed samples, indicating a preferential orientation on the (101) peak.

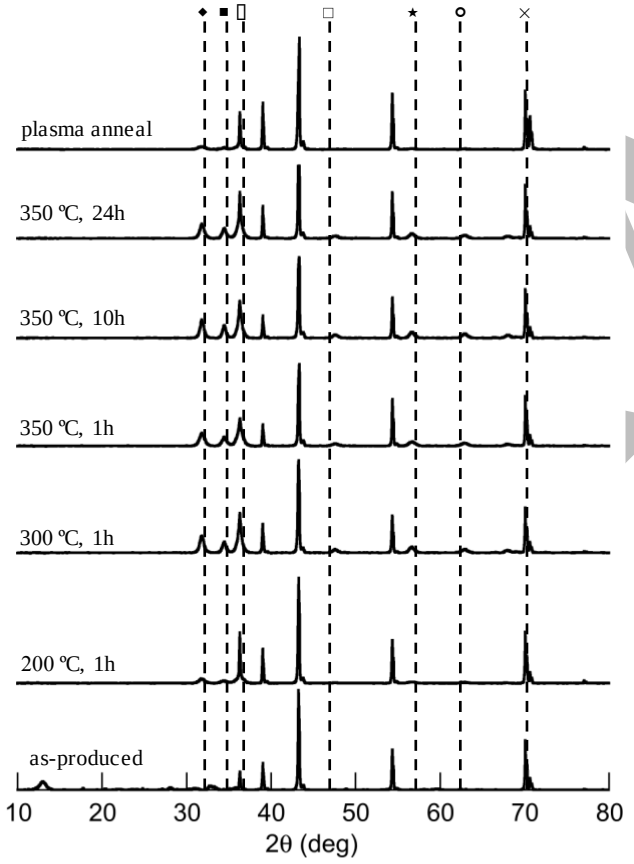

Fig. 2. XRD spectra for as-produced, thermally and plasma annealed ZnO-NFs. Key: ♦ ZnO (100); ■ ZnO (002); • ZnO (101); □ ZnO (102); ★ ZnO (110); ∘ ZnO (103); × ZnO (112); unlabelled peaks belong to the Zn metal substrate, with the exception of the small peak at 2θ = 13 deg, for which an attribution could not be found.

FESEM analysis for the as-produced, thermally and plasma annealed samples revealed that neither post-treatment affects the films' morphology prior to photocatalytic testing (Fig. 3a-c).

However, TEM analysis revealed significant changes in the morphology of individual nanowires resulting from the two annealing treatments (Fig. 3d-f). As-produced films (Fig. 3d) had a smooth surface with no individual crystallites observed. In thermally annealed ZnO, increases in crystallinity were observed in the TEM micrographs (Fig. 3e), with the formation of slit-type porosity, as reported elsewhere for thermally annealed ZnO nanowires produced with an ammonium carbonate, rather than potassium carbonate, as used here [22].

On the other hand, nanowires exposed to oxygen plasma (Fig. 3f) did not display any porosity on the surface, but rather showed an increase in surface roughness.

The changes produced in the ZnO-F by the thermal and plasma annealing processes resulted in an increase in the photocatalytic degradation of phenol of 33% and 46%, respectively, compared to the as-produced samples (Fig. 4). A significant change in the morphology of the as-produced and thermally annealed samples was observed after 4 hours of photocatalytic phenol degradation in the batch re-circulating reactor (Fig.1, configuration I), with the initial nanowire morphology changing to a flake-like appearance (cfr. Fig. 3a vs. 3g and Fig. 3b vs. 3h, respectively). In contrast, the plasma annealed samples retained the nanowire morphology (cfr. Fig. 3c vs Fig. 3i), with some secondary nanostructure growth observed. These morphological differences agree with the value of dissolved zinc in the solution after 4 hours, with the as-produced film having the highest value and the plasma annealed film the lowest (Table 1).

Table 1

Physico-chemical and kinetic parameters after 4h photocatalytic degradation of phenol: change in conductivity ((σ-σ_0)/ σ_0) and dissolved zinc [Zn], first order reaction rate constant (k) and final degradation (C/C_0).

	(σ-σ_0)/ σ_0 (-)	[Zn] (ppm)	k (h^{-1})	C/C_0 (-)	SEM Fig. 3
as-produced	4.5	5.4	0.10	0.24	g
thermally annealed	5.3	5.2	0.25	0.57	h
plasma annealed	6.7	3.8	0.31	0.70	i

As the photocatalytic reaction progresses, and depending on the pH of the solution, ZnO is dissolved into the electrolyte forming Zn^{2+}, $Zn(OH)_3^-$ or soluble $Zn(OH)_2$. Herein, the pH of the phenol solution was in the range of6.2 to 6.5, indicating that the predominant chemical species in solution was Zn^{2+}. According to the thermodynamic speciation of zinc (Fig. S2) [50], increases in the concentration of this ion causes the formation of insoluble $Zn(OH)_{2(s)}$ which precipitates resulting in the formation of new nanostructures (cfr. Fig. 3g).

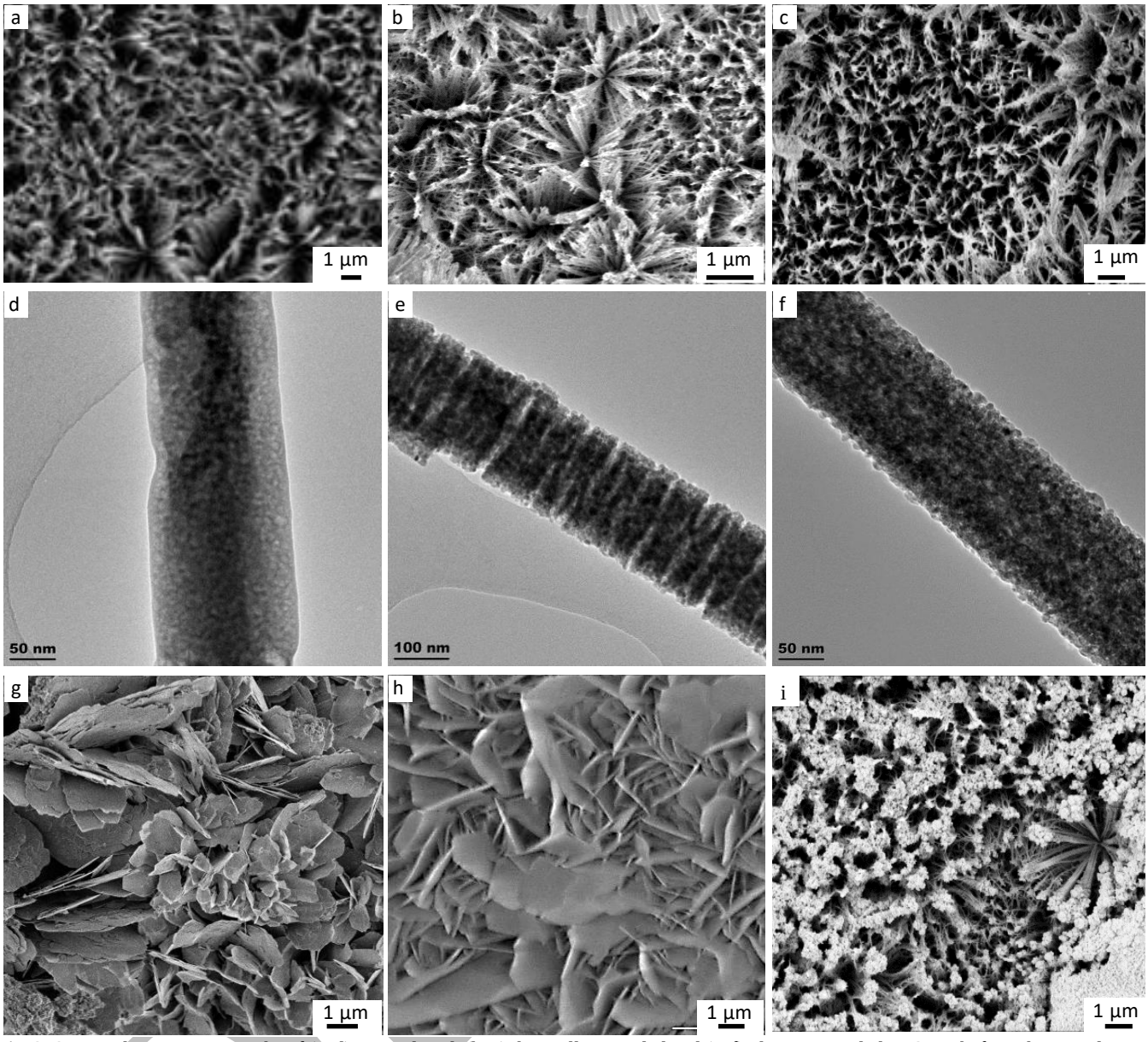

Fig. 3. SEM and TEM micrographs of (a, d) as-produced, (b, e) thermally annealed and (c, f) plasma annealed ZnO-FF before photocatalytic tests; SEM micrographs of (h) as-produced, (i) thermally annealed and (g) plasma annealed ZnO-FF after photocatalytic degradation of phenol for 4 hours.

The reduction in the dissolved Zn for the plasma annealed sample indicates less photo-corrosion of ZnO and therefore higher stability of the material that was expressed in a higher stability of the nanostructures. As such, the increase in the relative conductivity of the thermal and plasma annealed ZnO nanowire compared to the as-produced equivalent can be attributed to the enhancement of photocatalysis and thus higher production of phenol degradation products and CO_2 [40]. Oxygen plasma is also known to vary the hydrophobicity of the material [51], and suppresses the presence of chemisorption sites (oxygen deficiency sites) and oxygen vacancies [36], which can contribute to improving the photocatalytic activity of ZnO.

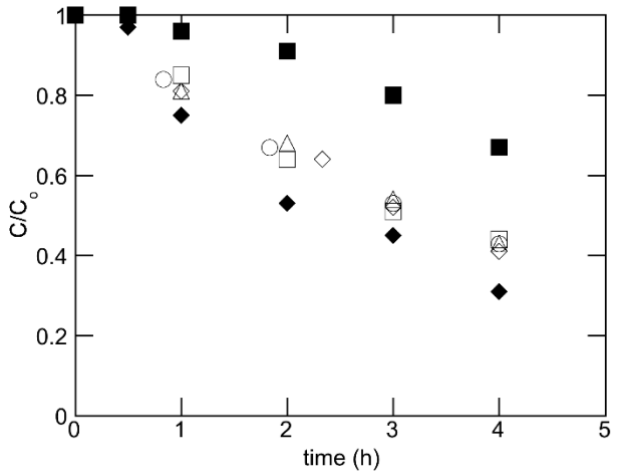

Fig. 4. Photocatalytic degradation of phenol using as-produced (■), thermally annealed (o – 30 min; Δ - 1h; □ - 18h; ◊ - 72h) and plasma (⬥) annealed ZnO-NFs.; error is below 5% for all data points.

3.1 Zn/ZnO wire catalyst reactor system

To test the ZnO nanowires in a flow configuration, a zinc wire rather than a flat film was used as a substrate on which to grow the nanowires. The non-planar geometry of the zinc wire substrate, however, introduced curvature-induced radial tension in the ZnO-W samples, which required some changes to the anodization procedure with respect to the flat ZnO-F photocatalysts. In particular, it was observed that the pre-anodization electropolishing treatment step led to significant embrittlement of the ZnO/Zn wire structures, making them unusable. Therefore, electropolishing was forgone, with the rest of the procedure remaining the same as for the flat-film samples. It is hypothesised here that this difference is due to the different morphology resulting from the wire forming process as opposed to the flat film [52]. The result, after post-anodization annealing, was the formation of a robust and uniform ZnO layer on the Zn wire (Fig. 5) that could be used under flow conditions (Fig. 1) without any measurable loss of oxide material.

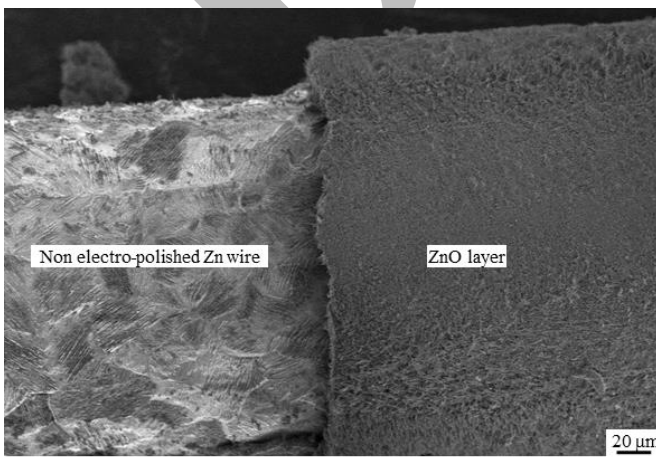

Fig. 5. SEM micrograph of a ZnO nanowire layer grown on Zn wire (ZnO-W).

The shape change had a significant effect on the photocatalytic activity of the ZnO-W, with the samples reaching similar degradation (~60%) in 1 hour (Fig. 6) rather than 4 h as for the ZnO-F catalysts (Fig. 4). The difference is even larger when one considers the UV dose received by the samples in the two reactor configurations (Table 2): if one compares the ZnO-F and ZnO-W both thermally annealed for 1h, after 1 hour of photocatalysis, the former has received a 40% higher UV dose while producing a phenol degradation that is 38% lower. Alternatively, for the same UV dose (2276 mJ/cm^2), the ZnO-W showed a 46% higher degradation than the ZnO-F (C/C_0 = 0.43 and 0.81, respectively).

Table 2
Phenol degradation and UV dose for ZnO-F and ZnO-W after 1h of photocatalytic degradation.

	ZnO-F, annealed				ZnO-W, annealed		
	thermal		plasma	Zn wire	thermal		plasma
	atm.	O_2 sat			atm.	O_2 sat	
UV dose [mJ/cm^2]	3192				2276		
C/C_0	0.81	0.88	0.75	0.59	0.43	0.35	N/A

Details of the calculations of the UV dose for all samples in Fig. 4 and Fig. 6 can be found in Table S1. Data for the UV dose and phenol degradation in Fig. 4 and Fig. 6 can be found in Tables S2 and S3, respectively. Fig. S3 directly compares the data from the two reactor configurations.

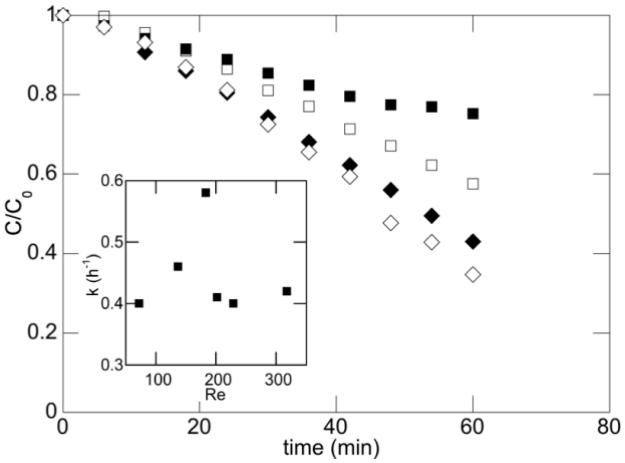

Fig. 6. Photocatalytic degradation of phenol in flow reactor by photolysis (■), untreated Zn wire (□), ZnO-W in air (⬥) and O_2-saturated atmosphere (◊); error is below 5% for all data points. Inset shows the first order reaction kinetics as a function of the flow rate (Reynolds number).

For the ZnO-W reactor configuration, significant degradation was also observed for the bare Zn wire. As previously discussed, electropolishing was forgone for this geometry, leaving a native and photoactive oxide layer on the surface of the wire. In addition, the cylindrical geometry of the wires prevented the ZnO-W

from being subjected to a uniform and consistent plasma annealing process, thus no data can be reported here.

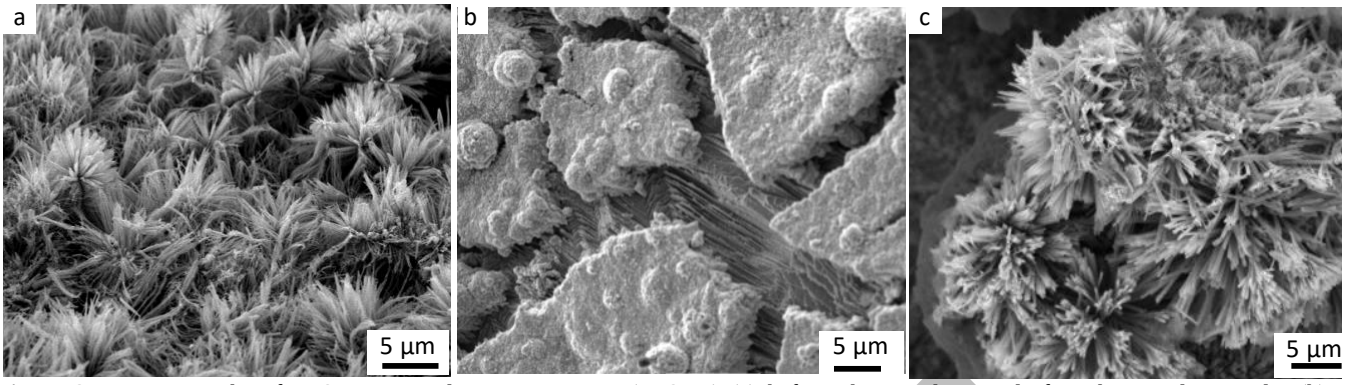

Fig. 7. SEM micrographs of ZnO nanowire layer on Zn wire (ZnO-W) (a) before photocatalysis and after photocatalysis under (b) atmospheric and (c) saturated oxygen environments.

The difference in performance between the two reactors can be convincingly attributed to hydrodynamic effects in the flow reactor [53]. In fact, changing the flow rate of the phenol solution significantly affected degradation, with an optimum at 250 mL/min (Fig. 6 inset). For the lower flow rates, increasing the flow rate increased the reaction kinetics, clearly showing that the process is in mass transfer-limited regime. This is a well-known effect, with the diffusion through the boundary layer at the liquid-catalyst interface limiting the rate of degradation [53]. As the flow rate increases, the laminar boundary layer thickness will decrease, thereby increasing the rate of mass transfer. A similar effect has been observed for the photocatalytic degradation of azo dyes using TiO_2 slurries [54]. At higher flow rates, when diffusion is no longer the limiting factor, adsorption of phenol on ZnO becomes the rate limiting step, with reaction kinetics becoming independent of flow rate (Fig. 6 inset). Comparable behaviour has been observed and fully modelled for phenol degradation in immobilised titania flow reactors [53]. Values well in excess of unity for the Peclet number (the ratio of convective to diffusional mass transfer), and a doubling of the Sherwood number (the ratio of convective mass transfer to the rate of diffusive mass transport) from 57 to 128, further support this analysis. All values and calculations are reported in Table S4 in the SI.

In Fig. 6, the effect of saturating the pollutant solution with oxygen is also shown. This results in increased degradation, from $C/C_0 = 0.43$ for the sample in air to 0.35 for the one under O_2 saturation. This can be attributed to an increased formation of superoxide radicals present in solution [18]. A similar effect was observed for the ZnO-F configuration (Table 2).

As already observed for the ZnO-F, the structure of the ZnO-W changed significantly during the photocatalytic experiments, with dissolution of the initial ZnO-W structures and re-deposition of nanosized super-structures onto the underlying nanowire surface when photocatalytic experiments were conducted under atmospheric conditions (cfr. Fig.7a and 7b). The secondary nanostructures observed are similar to those observed for the ZnO-F (cfr. Fig. 5 and Fig. 3a-b). However, under an oxygen-saturated environment, structural changes were significantly smaller (cfr. Fig. 7a and 7c). This difference in behaviour is attributed to a reduced dissolution of the zinc into the solution as a consequence of photocorrosion [18]. This interpretation is confirmed by the concentration of Zn in the solution after the photocatalytic flow reaction for 1 hour which is ~1 ppm for the ZnO-W under atmospheric conditions and ~0.1 ppm for the oxygen saturated experiment. Both values are significantly lower than those observed for ZnO-F in the batch system (Table 1). It is noted here that while the Zn concentration value under atmospheric conditions is one order of magnitude higher than the one obtained under oxygen-saturated environment, it is well below the 3 mg/L threshold recommended by the WHO, above which water assumes an unpleasant taste, greasy feel and opalescent colour [55].

3.2 Stability and reusability of the ZnO-W photocatalysts in flow

The re-usability of the ZnO-W wires was investigated by using the same sample over a period of three days and monitoring the photocatalytic degradation over five different irradiation cycles. The ZnO wire displayed very low dissolution of ZnO into the water, with maximum values over an hour period of 1 ppm. It was found that the ZnO-W was reusable, with no significant reduction in photocatalytic activity (Fig. 8). This level of performance is comparable to that observed for ZnO nanowires produced via hydrothermal synthesis [49]. The result in Fig. 8 is particularly promising, as both air and light have been known to deteriorate the oxide layer, leading to a reduction in photocatalytic effectiveness [56].

Finally, it is interesting to note that the change in nanostructure morphology does not significantly affect the photocatalytic behaviour of the ZnO-W.

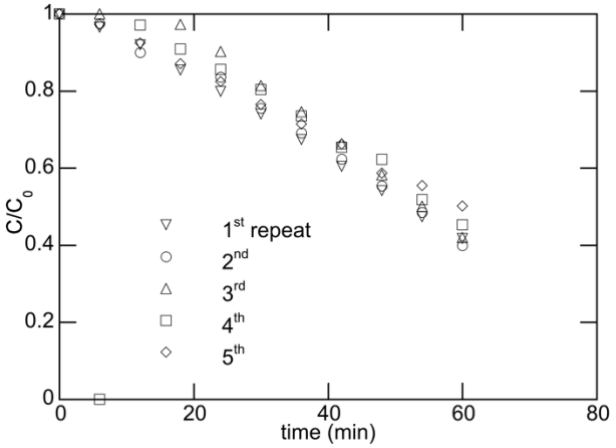

Fig. 8. Stability and reusability of the thermally annealed (1h) ZnO-W after five repeat uses over three days. The first reading was repeated five times with an error of less than 5%, and the following readings were taken once.

In fact, while surface area can be directly linked to photocatalytic activity in particle slurries [57], this is not the case for immobilized photocatalysts: in a previous publication, the authors have shown that photocatalytic activity can be quantitatively correlated to the light absorbance and crystal structure of the individual ZnO nanostructures, but not to their overall surface area or thickness, as one would normally expect for slurries of photocatalytic nanoparticles [40]. The present results appear to qualitatively support this view: while the super-structures might in fact be changing the thickness of the films and their surface area, they appear to not be blocking access to the underlying structure (Fig. 7b), thereby having a limited effect on light absorbance.

4. Conclusions

The effect of (i) post-treatment annealing, (ii) oxygen level and (iii) reactor configuration of ZnO nanowire films on photocatalytic activity was studied for the photocatalytic degradation of phenol. ZnO undergoes significant morphological changes during the photocatalytic reaction, with dissolution of zinc into the aqueous solution and concurrent reprecipitation of novel ZnO and $Zn(OH)_2$ nanostructures onto the original ZnO structure. The photocatalytic activity and stability of the films were enhanced by the thermal and oxygen plasma treatments. Switching from a flat film (batch reactor configuration) to a wire (tubular flow reactor) significantly enhanced the photocatalytic activity of the films. This is attributed to improved mass transfer for the same UV dose received by films, with a phenol degradation of 57%, compared to only 19% after 1 hour of exposure, for thermally annealed films. Oxygen plasma treatment and a saturated O_2 environment further enhanced the stability and resistance of the films. Finally, the ZnO-W films in the tubular flow reactor showed remarkable stability, with no loss in photocatalytic activity after 5 consecutive uses over 3 days. These results show that the combination of novel ZnO nanowire structures grown by anodization on zinc wires and a tubular flow reactor have high activity and can be an effective configuration for the degradation of pollutants in water.

Acknowledgements

The authors acknowledge the Centre for Sustainable Chemical Technologies of University of Bath for funding support (UK EPSRC EP/G03768X/1), Leeds EPSRC Nanoscience and Nanotechnology Research Equipment Facility-University of Leeds, and COLCIENCIAS–Colombia for supporting this project via the award of Francisco Jose de Caldas Scholarship to ARC. CMT was supported by an EPSRC funded Centre for Doctoral Training integrated Ph.D. studentship (EP/L016354/1). DM is supported by EPSRC (EP/P031382/1).
All data used in this manuscript is available from https://doi.org/10.15125/BATH-00675.

References

[1] Z.L. Wang, Zinc oxide nanostructures: growth, properties and applications, Journal of Physics: Condensed Matter, 16 (2004) R829-R858.
[2] A. Sapkota, A.J. Anceno, S. Baruah, O.V. Shipin, J. Dutta, Zinc oxide nanorod mediated visible light photoinactivation of model microbes in water, Nanotechnology, 22 (2011) 215703.
[3] P. Shukla, I. Fatimah, S. Wang, H.M. Ang, M.O. Tadé, Photocatalytic generation of sulphate and hydroxyl radicals using zinc oxide under low-power UV to oxidise phenolic contaminants in wastewater, Catalysis Today, 157 (2010) 410-414.
[4] M.X. Kang Han, Lianping Zhang, Lingpeng Yan, Junfeng Wei, Guoqi Ji, Qun Luo,, Y.H. Jian Lin, Chang-Qi Ma, Fully solution processed semi-transparent perovskite solar cells with spray-coated silver nanowires/ZnO composite top electrode, Solar Energy Materials and Solar Cells, 185 (2018) 399-405.
[5] D.T. G. Kartopu, , C. Ozcan,, W. Hadibrata,, P. Aurang,, S. Yerci,, V.B. H.E. Unalan, Y. Qu, L. Bowen, A.K. Gürlek, P. Maiello, R. Turan, S.J.C. Irvine, Photovoltaic performance of CdS/CdTe junctions on

ZnO nanorod arrays, Solar Energy Materials and Solar Cells, 176 (2018) 100-108.
[6] Y.K. Yohan Ko, Seong Young Kong, Sakeerali Cheeran Kunnan, Yongseok Jun, Improved performance of sol–gel ZnO-based perovskite solar cells via TiCl4interfacial modification, Solar Energy Materials and Solar Cells, 183 (2018) 157-163.
[7] J.S. Chang, J.K. Tan, S.N. Shah, A. Mateblowski, J. Strunk, P.E. Poh, M.N. Chong, Morphological tunable three-dimensional flower-like zinc oxides with high photoactivity for targeted environmental Remediation: Degradation of emerging micropollutant and radicals trapping experiments, Journal of the Taiwan Institute of Chemical Engineers, 81 (2017) 206-217.
[8] V. Vaiano, M. Matarangolo, J.J. Murcia, H. Rojas, J.A. Navío, M.C. Hidalgo, Enhanced photocatalytic removal of phenol from aqueous solutions using ZnO modified with Ag, Applied Catalysis B: Environmental, 225 (2018) 197-206.
[9] A. Ulyankina, I. Leontyev, M. Avramenko, D. Zhigunov, N. Smirnova, Large-scale synthesis of ZnO nanostructures by pulse electrochemical method and their photocatalytic properties, Materials Science in Semiconductor Processing, 76 (2018) 7-13.
[10] K.M. Lee, C.W. Lai, K.S. Ngai, J.C. Juan, Recent developments of zinc oxide based photocatalyst in water treatment technology: A review, Water Research, 88 (2016) 428-448.
[11] S. Sakthivel, B. Neppolian, M.V. Shankar, B. Arabindoo, M. Palanichamy, V. Murugesan, Solar photocatalytic degradation of azo dye: comparison of pho- tocatalytic efficiency of ZnO and TiO2, Solar Energy Materials and Solar Cells, 77 (2003) 65-82.
[12] F.D. Mai, C.C. Chen, J.L. Chen, S.C. Liu, Photodegradation of methyl green using visible irradiation in ZnO suspensions. Determination of the reaction pathway and identification of intermediates by a high-performance liquid chromatography–photodiode array-electrospray ionization-mass spectrometry, Journal of chromatography. A, 1189 (2008) 355-365.
[13] C.J. Lu, Y. Wu, F. Mai, W. Chung, C. Wu, W. Lin, C. Chen, Degradation efficiencies and mechanisms of the ZnO-mediated photocatalytic degradation of Basic Blue 11 under visible light irradiation, Journal of Molecular Catalysis A: Chemical, 310 (2009) 159-165.
[14] P. Spathis, I. Pouliost, The corrosion and photocorrosion of zinc and zinc oxide coatings, Corrosion Science, 37 (1995) 673-680.
[15] A.M. Ali, E.A.C. Emanuelsson, D.A. Patterson, Conventional versus lattice photocatalysed reactions: Implications of the lattice oxygen participation in the liquid phase photocatalytic oxidation with nanostructured ZnO thin films on reaction products and mechanism at both 254nm and 340nm, Applied Catalysis B: Environmental, 106 (2011) 323-336.
[16] J. Han, W. Qiu, W. Gao, Potential dissolution and photodissolution of ZnO thin films, Journal of hazardous materials, 178 (2010) 115-122.
[17] A.L. Rudd, C.B. Breslin, Photo-induced dissolution of zinc in alkaline solutions, Electrochimica Acta, 45 (2000) 1571-1579.
[18] A.M. Ali, E.A.C. Emanuelsson, D.A. Patterson, Photocatalysis with nanostructured zinc oxide thin films: The relationship between morphology and photocatalytic activity under oxygen limited and oxygen rich conditions and evidence for a Mars Van Krevelen mechanism, Applied Catalysis B: Environmental, 97 (2010) 168-181.
[19] J.L. Yang, S.J. An, W.I. Park, G.C. Yi, W. Choi, Photocatalysis Using ZnO Thin Films and Nanoneedles Grown by Metal-Organic Chemical Vapor Deposition, Advanced Materials, 16 (2004) 1661-1664.
[20] T. Kawano, H. Uchiyama, T. Kiguchi, S. Wada, H. Imai, Epitaxial growth of winding ZnO nanowires on a single-crystalline substrate, Journal of the Ceramic Society of Japan, 117 (2009) 255-257.
[21] A. Ramirez-Canon, D.O. Miles, P.J. Cameron, D. Mattia, Zinc oxide nanostructured films produced via anodization: a rational design approach, RSC Advances, 3 (2013) 25323-25330.
[22] D.O. Miles, P.J. Cameron, D. Mattia, Hierarchical 3D ZnO nanowire structures via fast anodization of zinc, Journal of Materials Chemistry A, (2015).
[23] S.G. Kumar, K.S.R.K. Rao, Zinc oxide based photocatalysis: tailoring surface-bulk structure and related interfacial charge carrier dynamics for better environmental applications, RSC Advances, 5 (2015) 3306-3351.
[24] E.a. Meulenkamp, Size Dependence of the Dissolution of ZnO Nanoparticles, The Journal of Physical Chemistry B, 102 (1998) 7764-7769.
[25] X. Zhang, J. Qin, R. Hao, L. Wang, X. Shen, R. Yu, S. Limpanart, M. Ma, R. Liu, Carbon-Doped ZnO Nanostructures: Facile Synthesis and Visible Light Photocatalytic Applications, The Journal of Physical Chemistry C, 119 (2015) 20544-20554.
[26] M.M. Ba-abbad, A. Amir, H. Kadhum, A. Bakar, M.S. Takriff, Visible light photocatalytic activity of Fe 3 + -doped ZnO nanoparticle prepared via sol – gel technique, Chemosphere, 91 (2013) 1604-1611.
[27] O. Yayapao, T. Thongtem, A. Phuruangrat, S. Thongtem, Ultrasonic-assisted synthesis of Nd-doped ZnO for photocatalysis, Materials Letters, 90 (2013) 83-86.
[28] S. Kuriakose, B. Satpati, S. Mohapatra, Enhanced photocatalytic activity of Co doped ZnO nanodisks and nanorods prepared by a facile wet chemical method, Physical chemistry chemical physics, 16 (2014) 12741-12749.

[29] R. Mohan, K. Krishnamoorthy, S.-J. Kim, Enhanced photocatalytic activity of Cu-doped ZnO nanorods, Solid State Communications, 152 (2012) 375-380.
[30] M. Ahmad, E. Ahmed, Y. Zhang, N.R. Khalid, J. Xu, M. Ullah, Z. Hong, Preparation of highly efficient Al-doped ZnO photocatalyst by combustion synthesis, Current Applied Physics, 13 (2013) 697-704.
[31] B. Bayraktaroglu, K. Leedy, R. Bedford, High temperature stability of postgrowth annealed transparent and conductive ZnO:Al films, Applied Physics Letters, 93 (2008) 022104-022104.
[32] Z. Hu, Q. Chen, Z. Li, Y. Yu, L.M. Peng, Large-Scale and Rapid Synthesis of Ultralong ZnO Nanowire Films via Anodization, Journal of Physical Chemistry C, 114 (2010) 881-889.
[33] N. Samir, D.S. Eissa, N.K. Allam, Self-assembled growth of vertically aligned ZnO nanorods for light sensing applications, Materials Letters, 137 (2014) 45-48.
[34] P.F. Cai, J.B. You, X.W. Zhang, J.J. Dong, X.L. Yang, Z.G. Yin, N.F. Chen, Enhancement of conductivity and transmittance of ZnO films by post hydrogen plasma treatment, Journal of Applied Physics, 105 (2009) 1-6.
[35] C.-H. Hsu, D.-H. Chen, CdS nanoparticles sensitization of Al-doped ZnO nanorod array thin film with hydrogen treatment as an ITO/FTO-free photoanode for solar water splitting, Nanoscale Research Letters, 7 (2012) 593-593.
[36] M. Liu, H.K. Kim, Ultraviolet detection with ultrathin ZnO epitaxial films treated with oxygen plasma, Applied Physics Letters, 84 (2004) 173-173.
[37] B. Angadi, H.C. Park, H.W. Choi, J.W. Choi, W.K. Choi, Oxygen plasma treated epitaxial ZnO thin films for Schottky ultraviolet detection, Journal of Physics D: Applied Physics, 40 (2007) 1422-1425.
[38] X.Q. Meng, D.X. Zhao, J.Y. Zhang, D.Z. Shen, Y.M. Lu, L. Dong, Z.Y. Xiao, Y.C. Liu, X.W. Fan, Wettability conversion on ZnO nanowire arrays surface modified by oxygen plasma treatment and annealing, Chemical Physics Letters, 413 (2005) 450-453.
[39] E. Lee, S. Kim, S. Heo, J. Lee, Effects of oxygen plasma post-treatment on the structural, electrical and optical properties of Ga-doped ZnO films, Journal of the Korean Physical Society, 67 (2015) 1767-1772.
[40] A. Ramirez-Canon, M. Medina-Llamas, M. Vezzoli, D. Mattia, Multiscale design of ZnO nanostructured photocatalysts, Physical Chemistry Chemical Physics, 20 (2018) 6648--6656.
[41] S. Lathasree, A.N. Rao, B. SivaSankar, V. Sadasivam, K. Rengaraj, Heterogeneous photocatalytic mineralisation of phenols in aqueous solutions, Journal of Molecular Catalysis A: Chemical, 223 (2004) 101-105.
[42] J. Wenk, S. Canonica, Phenolic antioxidants inhibit the triplet-induced transformation of anilines and sulfonamide antibiotics in aqueous solution, Environ Sci Technol, 46 (2012) 5455-5462.
[43] A. Leifer, The Kinetics of Environmental Aquatic Photochemistry: Theory and Practice, USA, 1988.
[44] D.S. Grzegorz, Highly ordered anodic porous alumina formation by self-organized anodizing, in: V.C.H.V.G. Wiley, W.G. Co. KgaA (Eds.), Germany, 2008.
[45] A. Eftekhari, Nanostructured Materials in Electrochemistry, in, Wiley-VCH, Weinheim, 2008.
[46] Z.B. Fang, Z.J. Yan, Y.S. Tan, X.Q. Liu, Y.Y. Wang, Influence of post-annealing treatment on the structure properties of ZnO films, Applied Surface Science, 241 (2005) 303-308.
[47] P.-H. Shih, H.-J. Hung, Y.-R. Ma, S.-Y. Wu, Tuning the dimensionality of ZnO nanowires through thermal treatment: An investigation of growth mechanism, Nanoscale research letters, 7 (2012) 354-354.
[48] V. Subramanian, P.V. Kamat, E.E. Wolf, Mass-Transfer and Kinetic Studies during the Photocatalytic Degradation of an Azo Dye on Optically Transparent Electrode Thin Film, Industrial & Engineering Chemistry Research, 42 (2003) 2131-2138.
[49] Y.G. Habba, M. Capochichi-Gnambodoe, L. Serairi, Y. Leprince-Wang, Enhanced photocatalytic activity of ZnO nanostructure for water purification, physica status solidi (b), 253 (2016) 1480-1484.
[50] T. William, J. Albrecht, J. Addai-Mensah, D. Fornasiero, Effect of pH, Concentration and Temperature on Copp er and Zinc Hydroxide Formation/Precipitation in Solution, in: Chemeca 2011, Sydney, Australia, 2011, pp. 2100-2110.
[51] X.Q. Meng, D.X. Zhao, J.Y. Zhang, D.Z. Shen, Y.M. Lu, L. Dong, Z.Y. Xiao, Y.C. Liu, X.W. Fan, Wettability conversion on ZnO nanowire arrays surface modified by oxygen plasma treatment and annealing, Chemical Physics Letters, 413 (2005) 450-453.
[52] Y.R.S. ARCHANA KAR, VAIDYANATHAN (RAVI) SUBRAMANIAN, Improved Photocatalytic Degradation of Textile Dye Using Titanium Dioxide Nanotubes Formed Over Titanium Wires, Environ. Sci. Technol., 43 (2009) 3260–3265.
[53] H. de Lasa, B. Serrano, M. Salaices, Photocatalytic Reaction Engineering, Springer, New York, 2005.
[54] Vaidyanathan Subramanian, ‡ Prashant V. Kamat,† and Eduardo E. Wolf, Mass-Transfer and Kinetic Studies during the Photocatalytic
Degradation of an Azo Dye on Optically Transparent Electrode Thin
Film, Ind. Eng. Chem. Res., 42 (2003) 2131-2138.
[55] WHO, Unicef, Joint Monitoring Programme (JMP) for Water Supply and Sanitation, in, 2012.

[56] A.B. Djurišić, X. Chen, Y.H. Leung, A. Man Ching Ng, ZnO nanostructures: growth, properties and applications, Journal of Materials Chemistry, 22 (2012) 6526.
[57] R. van Grieken, J. Marugán, C. Sordo, C. Pablos, Comparison of the photocatalytic disinfection of E. coli suspensions in slurry, wall and fixed-bed reactors, Catalysis Today, 144 (2009) 48-54.